Available online at www.sciencedirect.com
SCIENCE DIRECT®
Journal of Sound and Vibration 262 (2003) 219–244
JOURNAL OF SOUND AND VIBRATION
www.elsevier.com/locate/jsvi

# Transient vibration phenomena in deep mine hoisting cables. Part 1: Mathematical model

S. Kaczmarczyk[a,*,1], W. Ostachowicz[b]

[a] *School of Mechanical Engineering, University of Natal, Durban 4041, South Africa*
[b] *Institute of Fluid Flow Machinery, Polish Academy of Sciences, 14 Fiszera Street, 80-952 Gdansk, Poland*

Received 30 May 2001; accepted 2 May 2002

**Abstract**

The classical moving co-ordinate frame approach and Hamilton's principle are employed to derive a distributed-parameter mathematical model to investigate the dynamic behaviour of deep mine hoisting cables. This model describes the coupled lateral–longitudinal dynamic response of the cables in terms of non–linear partial differential equations that accommodate the non-stationary nature of the system. Subsequently, the Rayleigh–Ritz procedure is applied to formulate a discrete mathematical model. Consequently, a system of non-linear non-stationary coupled second order ordinary differential equations arises to govern the temporal behaviour of the cable system. This discrete model with quadratic and cubic non-linear terms describes the modal interactions between lateral oscillations of the catenary cable and longitudinal oscillations of the vertical rope. It is shown that the response of the catenary–vertical rope system may feature a number of resonance phenomena, including external, parametric and autoparametric resonances. The parameters of a typical deep mine winder are used to identify the depth locations of the resonance regions during the ascending cycles with various winding velocities.


## 1. Introduction

Ropes and cables are among the oldest tools and structural elements used in engineering. Thus, it is not surprising that the behaviour and mechanical properties of these elements have been studied extensively for many hundreds of years, and these studies have resulted in the introduction of a number of well-known theories and techniques. For example, Stevin in 1586 instituted the

*Corresponding author. Tel.: +44-1604-893158; fax: +44-1604-792650.
*E-mail address:* stefan.kaczmarczyk@northampton.ac.uk (S. Kaczmarczyk).
[1] Presently at the School of Technology & Design, University College Northampton, St. George's Avenue, Northampton NN2 6JD, UK.

0022-460X/03/$ - see front matter 
doi:10.1016/S0022-460X(02)01137-9

triangle of forces by experimenting with loaded strings, Beeckman in about 1615 solved the suspension bridge problem, and James and John Bernoulli between 1690 and 1691 established the foundations of the catenary theory [1].

Cables, due to their low bending and torsional stiffness, and due to their ability to resist relatively large axial loads, have been widely used in towing operations, to support structures, to conduct signals, and to carry payloads. In this latter application, cables have played a vital role in industrial hoisting installations, and particularly in deep mine hoist systems. A common arrangement in these systems, referred to as a single-drum system, is shown in Fig. 1. It comprises a driving winding drum, a steel wire cable, a sheave mounted in headgear, and a conveyance. The cable passes from the drum over the sheave, forming a horizontal or inclined catenary, to the conveyance constrained to move in a vertical shaft, and forms the vertical rope hanging below the headsheave. A cable storage mechanism on the winder drum is applied in order to facilitate a uniform coiling pattern. This system can be treated principally as an assemblage of two connected interactive, continuous substructures, namely of the catenary and of the vertical rope, with the sheave acting as a coupling member, and with the winder drum regarded as an energy source. An important feature of this systems is that the hoisting cable is of time-varying length. However, the variation is small over a time period corresponding to the fundamental frequency of the system and the length is said to vary slowly. Consequently, the dynamic characteristics of the system vary slowly during the wind, rendering the system non-stationary.

Other different configurations of the hoisting system are used in various industries. For example, double-drum systems operate at higher depths. These systems are formed essentially by two mechanically coupled single-drum systems, with one system acting as the overlay and the other as the underlay installation. However, the majority of hoisting systems usually can be modelled as a simple single-drum installation. The dynamic behaviour of this typical hoisting

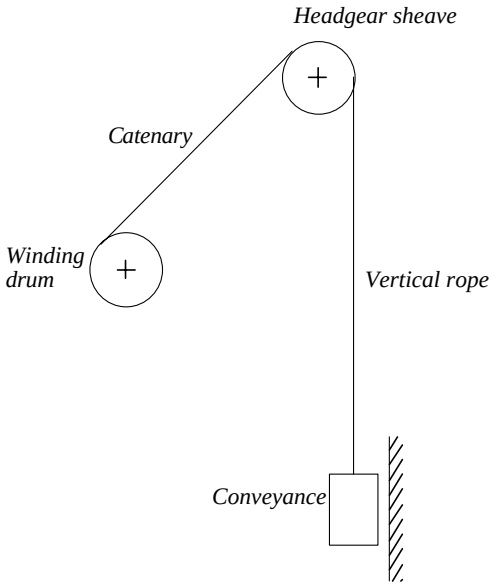


Fig. 1. A single-drum hoisting installation.

installation, hereafter referred to as the catenary–vertical rope system, is addressed in this study. The importance of this subject cannot be overestimated, especially in the context of the mining industry, where the safety of personnel and profitability rely on stable designs.

Thus, it is not surprising that numerous aspects of the dynamic behaviour of hoisting cables, in particular in elevators and in mine hoists, have been studied in the past. In early research attempts, the scope of the studies was limited to the longitudinal dynamic behaviour of a vertical rope of fixed length with end mass [2–5]. More recently, Goroshko and Savin [6,7] studied longitudinal and transverse oscillations of a vertical rope with slowly varying length. In this study, the dynamic response due to the acceleration and deceleration inertial loads was investigated applying integro-differential equations with time-varying intervals and kernels. Following the fundamental concepts for non-linear oscillating systems with slowly varying parameters established by Mitropolskii [8], they developed an innovative and efficient approach to model one-dimensional systems with time-varying length. Kotera [9] treated free and forced vibrations of a vertical rope with time-varying length and a concentrated mass attached to its end. In this research, an analytical method based on the method of separation of variables was proposed to solve the problem. Marczyk and Niziol [10] analyzed the influence of longitudinal oscillations on the lateral behaviour of vertical hoisting ropes, and applied methodology developed by Goroshko and Savin [6] to construct an asymptotic solution to analyze parametric resonance occurring in the system. Klich [11] considered the non-stationary dynamics of winding ropes together with the driving electrical system. The problem of optimal control of the driving system was analyzed and modelling techniques were discussed. Mankowski [12] carried out a computer simulation of the dynamic behaviour of a typical hoisting cable system. A lumped-mass model of the system was developed to describe the lateral motions of the catenary cable and the longitudinal dynamics of the vertical rope due to a kinematic excitation arising at the winder drum. Constancon [13] re-addressed the problem as stated by Mankowski and proposed a distributed-parameter model describing the lateral–longitudinal dynamics of the system applying the theory of travelling cables formulated by Perkins and Mote Jr. [14]. In this study, a stationary model was used to investigate the stability of linear steady state motion in the context of the non-linear equations of motion of the system by applying a harmonic balance method, and a laboratory experiment was conducted to verify the results. Besides, the non-stationary nature of the system was accounted for in a numerical simulation of equations of motion.

More recently, Kumaniecka and Niziol [15] presented interesting results on parametric resonance in a longitudinal–transverse model of a vertical rope with dry friction, material non-linearity and slowly varying length. They applied the method of harmonic balance to identify parametric combination resonance regions, and found that as a result of non-linear coupling between the longitudinal and transverse modes, parametric resonance was possible, but only at high amplitudes of longitudinal motion. Non-stationary parametric resonance was considered also by Terumichi et al. [16]. They analyzed passage through resonance in a model of a high-rise building elevator and studied vibrations of a vertical string with time-varying length and a mass–spring system attached at the lower end. The upper end was subject to a harmonic motion. Influence of the axial velocity on the transverse amplitude was examined and was shown that the amplitude decreased when the velocity was increased.

In this paper, the coupled lateral–longitudinal dynamic response of the catenary–vertical rope system during a winding cycle is investigated. The classical moving frame approach and

Hamilton's principle are applied to formulate the mathematical model of the system. The dynamic response is defined in terms of a set of non-linear partial differential equations that accommodates the fundamental non-stationary nature of the hoisting installation. This enables one to analyze the non-linear transient resonance phenomena occurring in the system.

## 2. Vibration model

The dynamic response of hoisting cables is usually classified as lateral and longitudinal vibrations in the catenary and the vertical rope [17]. Steel wire cables can also respond in torsion to applied axial load, and the torsional response is coupled with the longitudinal response [7,18]. The torsional vibration may occur in cables of certain construction, for example in the triangular strand winding ropes. The wires in the strands in these ropes are bent over a triangular centre wire, as shown in Fig. 2. Due to the large effective cross-sectional area, this type of rope is suitable for multi-layer coiling on drum hoists [19], and has become the industry norm for mine hoisting installations. However, it was shown by Hamilton and Greenway [20] that the effect of the torsional coupling on the dynamic response of the triangular strand rope was not significant, and that it can be neglected in the dynamic analysis of hoisting cables.

The winding cable vibrations are caused by various sources of excitation present in the system. The most significant sources are load due to the winding cycle acceleration/deceleration profile and a mechanism applied on the winder drum surface in order to achieve a uniform coiling pattern. In this mechanism, the path of the first cable layer in contact with the drum is prescribed in such a way that the pattern for the following layers is also imposed. Thus, typically the winder drum surface is covered by parallel circular grooves with two diametrically opposed cross-over zones per drum circumference, as shown in Fig. 3. In this arrangement, $R_d$ denotes the drum radius, $d$ is the cable diameters, and $\beta$ represents the angle defining the diametrical arc

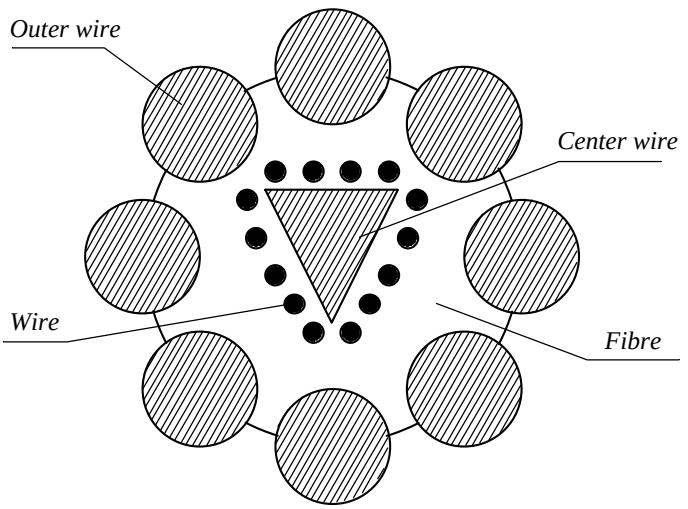


Fig. 2. A strand cross-section of the triangular strand winding rope.

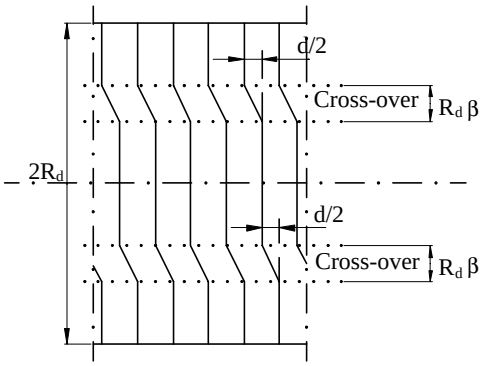


Fig. 3. The winder drum cross-over zones.

corresponding to the cross-over zone. Each zone offsets the grooves by half a cable diameter until the cable reaches the drum flange. Then a guide forces a layer change, and the spooling continues in the opposite direction. In this process, when the cable passes through a cross-over, additional lateral and axial displacements relative to the nominal transport motion occur. Other sources may include motions of the headgear, shape imperfections and eccentricity of the winder drum and sheave, misalignment in the shaft steelwork, and aerodynamic effects. Some of these sources may be manifested as *external excitations* in the system, and appear as inhomogeneities in the governing differential equations, and some may lead to *parametric excitation*s, which appear as coefficients in the governing differential equation*s*.

The lateral vibration is usually associated with the catenary. It leads to the catenary whirling motion referred to as "rope whip". This resonance phenomenon may cause miscoiling at the winder drum, may lead to the cable jumping out of the sheave groove, and also to damage caused by impact of the cable against the frame of the headgear structure or against the winding house openings. It should be noted that the catenary section of the hoisting cable may be treated as a taut string element, and many dynamic phenomena reported as occurring in resonant motions of strings are pertinent to the catenary dynamic behaviour. These have been studied extensively [21–30], and include primary, secondary and combination external resonances, principal and combination parametric resonances, and internal *(autoparametric)* resonances.

The primary sources of the catenary oscillations are the periodic excitation due to the coil cross-over motion and the layer change pulses. The transverse vibrations are also noticeable in the vertical rope, mainly at the upper level of the shaft. Mankowski [12] noted that they were of small amplitude and of a wide range of frequencies, and may be induced by the misalignment in the shaft steelwork or irregularities at the sheave. Also, the rope transverse vibration may result due to a parametric excitation when the dynamic tension fluctuations in the catenary are transmitted to the vertical section via the headsheave.

The longitudinal vibration is usually associated with the vertical rope. This vibration affects the motion of the conveyance introducing the so-called "yo-yo" type oscillation, and may also be observed at the headsheave. The inertial load due to the winding cycle acceleration/deceleration profile is primarily responsible for the longitudinal transient response. Longitudinal pulses arising due to coil cross-over zones, and also due to the cable layer change at the winder drum, cause additional longitudinal response.

Interactions between various types of vibration within the catenary and the vertical rope exist. The sheave inertial coupling between the two subsystems also facilitates extensive interactions between the catenary and the vertical rope motions. The nature of these interactions is strongly non-linear. The lateral vibration of the catenary induces the longitudinal oscillations in the vertical system and vice versa. Also, significant coupling between the lateral vibration of the vertical system and the lateral motion of the catenary can be observed [13].

The hoisting cable system is essentially a non-linear non-stationary oscillatory system with slowly varying natural frequencies and mode shapes, which is due to time-varying length of the vertical rope and consequently due to slow variation of the mean catenary tension. Furthermore, it is known that the natural frequency of each mode of an axially moving continuous member decreases with the transport speed [31]. Thus, the catenary, essentially representing a translating string, has also its natural modes influenced by the winding velocity. It is evident that the dynamic behaviour of this system is very complex, and a passage through various resonance conditions may occur during its operation.

An efficient model which adequately accounts for the fundamental features, to simulate the dynamic response of the system, is of importance in the present analysis. Two main approaches can be distinguished in modelling of the dynamics of cable-hoisting systems. In the first, a motion of the winder drum is assumed to be prescribed, usually through a known velocity or acceleration profile. In this model, the driving system, usually an electric DC or AC motor, is not taken into consideration. In the second approach, in order to define the transportation motion, the dynamic characteristics of an external source of power are included into the studies. This means that additional differential equations describing the driving motor dynamic characteristics must be added to the governing differential equations of the system which result in additional degrees of freedom. However, the advanced control systems used in modern installations allow accurately prescribed velocity and acceleration profiles of the winder drum to be realized. Therefore, the first approach is often well justified, in which the system power supply is considered to be unlimited. The winder drum is then treated as an *ideal source of energy*, and the system is referred to as *an ideal system*.

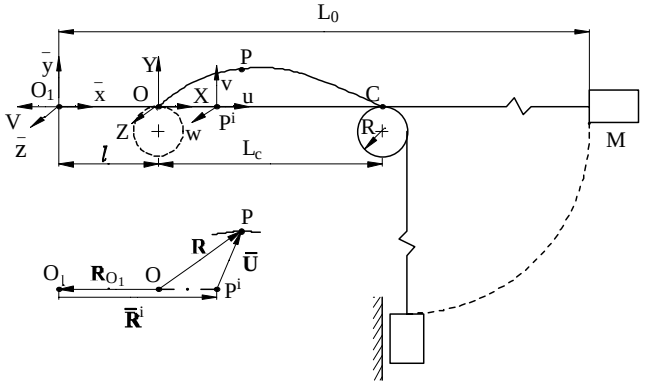


Fig. 4. A model of the catenary–vertical rope hoisting system.

A model of the cable-hoisting system is represented in Fig. 4. In this model, the cable is divided into a horizontal catenary[2] of length $OC=L_c$ passing over a sheave of radius $R$, and of mass moment of inertia $I$, and into a vertical rope with a mass $M$, representing the conveyance mass and payload, attached to its bottom end. The end $O_1$ of the cable is moving with a prescribed winding velocity $V(t)$ due to the cable being coiled onto a rotating cylindrical drum, so that the entire system translates axially, with the mass $M$ being constrained in a lateral direction. The section $l=OO_1$ represents a time-varying length of this part of the cable that is already coiled onto the winder drum. The cable has a constant effective cross-sectional area $A$, a constant mass per unit length $m$, and an effective Young's modulus $E$.

In order to describe the oscillations of the cable, the classical moving frame approach is applied [32]. Two frames of reference are established: a coordinate system $O_1\bar{x}\,\bar{y}\,\bar{z}$ attached to, and moving with the upper end of the cable, and a stationary inertial system $OXYZ$. The following fundamental assumptions are made: (1) the system is an ideal system; (2) the cable material is uniform; (3) the winder drum, headgear, sheave, conveyance, and shaft steelwork are perfectly rigid; (4) there is no cable slip on the winder drum or across the sheave; (5) the effect of torsional coupling on the dynamic response is not significant and can be neglected; (6) the catenary cable is taut and flat in its initial equilibrium configuration[3]; (7) only longitudinal motion in the vertical subsystem is admitted.

The dynamic deformed position $P$ of an arbitrary section of the cable during its motion is defined in the inertial frame by the position vector

$$\mathbf{R}(s,t)=\mathbf{R}_{O_1}(t)+\bar{\mathbf{R}}^i(s)+\bar{\mathbf{U}}(s,t), \tag{1}$$

where $s$ denotes the Lagrangian (material) co-ordinate of $P^i$, representing the dynamically undeformed position of the cable section, and measured from the origin $O_1$. In this representation the axial transport motion is treated as essentially an overall rigid-body translation, and the dynamic elastic deformations are referred to the moving frame associated with this motion. The entire cable is prestressed, and all dynamic characteristics of the cable are functions of the independent variables $(s,\ t)$, with $s$ being referred to the prestressed state and the moving frame. The vector $\mathbf{R}_{O_i}(t)=[-l,\ 0,\ 0]^{\mathrm{T}}$ represents the position of the origin $O_1$ in the inertial frame, $\bar{\mathbf{R}}^i=[s,\ 0,\ 0]^{\mathrm{T}}$ defines the initial reference position $P^i$ of the cable section, $\bar{\mathbf{U}}=[u(s,t),\ v(s,t),\ w(s,t)]^{\mathrm{T}}$ is the dynamic displacement vector from the reference configuration, with $u,\ v$, and $w$ representing the longitudinal, in-plane lateral, and out-of-plane lateral motion, respectively. The upper bar denotes vectors referred to the moving frame. Upon assuming that the modulus $E$ of the cable material is high, the strain of the cable wound around the drum can be neglected [7], and the length $l$ is then given by

$$l(t)=l(0)\pm\int_0^t V(\xi)\mathrm{d}\xi, \tag{2}$$

[2] Using the justification that the effect of gravity due to a catenary inclination is small in comparison to the total quasi-static tension, this model is valid also in the case of a system with an incline catenary cable. This approximation results in a uniform mean catenary tension.

[3] The catenary profile lies very close to the chord between the drum and the sheave under the normal loading conditions due to the payload and mass of the vertical cable. Thus, the catenary tension is high and it is assumed that the catenary cable forms the limiting configuration of a taut string, with its initial curvature being, by definition, zero.

where signs "+" and "−"correspond to ascending and descending, respectively, and $l(0)$ is the initial length[4].

Taking into consideration the assumption that there is no lateral motion in the vertical rope, and denoting the longitudinal dynamic deflection in the catenary and in the vertical rope as $u_c(s,\ t)$ and $u_v(s,\ t)$, respectively, the deformed position vector is defined as

$$\mathbf{R} = \left\{ \begin{array}{c} [s + u_c(s,t) - l, v(s,t),\ w(s,t)]^{\mathrm{T}}, l \leqslant s \leqslant L_1, \\ [s + u_v(s,t) - l, 0, 0)]^{\mathrm{T}}, L_1 \leqslant s \leqslant L_0, \end{array} \right\}, \tag{3}$$

where $L_1 = l + L_c$, and $L_0$ denotes the total length of the cable in the reference configuration. The continuity of deflection across the sheave requires $u_c(L_1, t) = u_v(L_1, t) = u_1$, and the dynamic elastic deflection at the vertical rope bottom end is $u_2 = u_v(L_0, t)$. The velocity vector of a cable particle $P$ is then determined as

$$\dot{\mathbf{R}} = \left\{ \begin{array}{c} \mathbf{V}_c = \left[u_{c,t}(s,t) - \dot{l},\ v_{,t}(s,t), w_{,t}(s,t)\right]^{\mathrm{T}}, l \leqslant s \leqslant L_1 \\ \mathbf{V}_u = \left[u_{v,t}(s,t) - \dot{l}, 0, 0\right]^{\mathrm{T}}, L_1 \leqslant s \leqslant L_0 \end{array} \right\}, \tag{4}$$

where the overdot indicates total differentiation with respect to time, and $(\ )_{,\mathrm{t}}$ denotes partial derivatives with respect to time.

This Lagrangian formulation enables one to derive efficiently the equations of motion of the catenary–vertical rope assembly. The details of the derivation are presented in what follows.

## 3. Equations of motion

### 3.1. Free motion

The equations governing the free undamped response of the system can be derived by applying the variational approach of analytical mechanics. In this approach, Hamilton's principle can be used which requires that the time integral of the difference between the kinetic and potential energies shall be stationary. Hence, the Hamilton formulation applied to the catenary–vertical rope system yields

$$\int_{\mathrm{t}_1}^{\mathrm{t}_2} (\delta E - \delta \Pi_e - \delta \Pi_{\boldsymbol{g}}) \mathrm{d}t = 0, \tag{5}$$

where $E$, $\Pi_e$, and $\Pi_{\boldsymbol{g}}$ denote the system kinetic energy, the cable elastic strain energy, and the system gravitational potential energy, respectively. Upon assuming that the dynamic deflections

[4] The exact geometric relationship should read $l(t) + u(l,t) = \pm \int_0^t V(\xi)\mathrm{d}\xi$, where $u(l,\ t)$ denotes a longitudinal deformation of the cable wound around the drum. This expression can be differentiated with respect to t, so that $\dot{l}(t) = V(t)/(1 + (\partial u(l,t)/\partial s))$, and consequently $l(t) = l(0) \pm \int_0^t (V(\xi)/(1 + \partial u(l,\xi)/\partial s)\mathrm{d}\xi$. For cables of high Young's modulus, for example for steel wire cables, the longitudinal strain is small, namely $\partial u(l,t)/\partial s \ll 1$, so that the approximation (2) can be applied.

of section $OO_1$ of the cable can be neglected, the kinetic energy of the system is expressed as

$$E = \int_l^{L_1} \hat{E}_c(u_{c,t}, v_{,t}, w_{,t})\mathrm{d}s + \int_{L_1}^{L_0} \hat{E}_v(u_{v,t})\mathrm{d}s + E_s(\dot{q}_1) + E_M(\dot{q}_2), \tag{6}$$

where

$$\hat{E}_c = \tfrac{1}{2}m\mathbf{V}_c \bullet \mathbf{V}_c, \quad \hat{E}_v = \tfrac{1}{2}m\mathbf{V}_v \bullet \mathbf{V}_v, \quad \hat{E}_s = \frac{1}{2}\frac{I}{R^2}\dot{q}_1^2, \quad \hat{E}_M = \tfrac{1}{2}M\dot{q}_2^2, \tag{7a-d}$$

where $\dot{q}_1 = u_{v,t}(L_1, t) - \dot{l}$, and $\dot{q}_2 = u_{v,t}(L_0, t) - \dot{l}$, with $q_1$, $q_2$ representing the total displacements at the sheave and at the conveyance, respectively.

The elastic strain energy of the cable is

$$\Pi_e = \Pi_e^i + \int_l^{L_1} \hat{\Pi}_c(u_{c,s}, v_{,s}, w_{,s})\mathrm{d}s + \int_{L_1}^{L_0} \hat{\Pi}_v(u_{v,s})\mathrm{d}s, \tag{8}$$

where $\Pi_e^i$ is the strain energy in the reference prestressed configuration, and

$$\hat{\Pi}_c = (T_c^i + \tfrac{1}{2}EA\varepsilon_c)\varepsilon_c, \quad \hat{\Pi}_v = (T_v^i + \tfrac{1}{2}EA\varepsilon_v)\varepsilon_v, \tag{9a, b}$$

where $\varepsilon_c$ and $\varepsilon_v$ represent the strain measure in the catenary section and the vertical section of the cable, respectively, $T_c^i$, and $T_v^i$ represent the quasi-static tension in the catenary, and in the vertical cable in the reference configuration, respectively. Using the *large displacement approach* [33], the catenary strain measure resulting from *Green's symmetric strain tensor* is given by

$$\varepsilon_c = u_{c,s} + \tfrac{1}{2}(v_{,s}^2 + w_{,s}^2), \tag{10}$$

where $(\,)_{,s}$ denotes partial differentiation with respect to $s$. In this non-linear strain measure, large displacements generated by the rotations are accounted for, with the assumption that the axial deformations remain small. The strain measure in the vertical rope is given in the classical linear straight bar form, where both rotations and displacements are assumed to be small, namely

$$\varepsilon_v = u_{v,s}. \tag{11}$$

The gravitational potential energy of the cable expressed in terms of the dynamic deflections is given by

$$\Pi_g = \Pi_g^i - \int_{L_1}^{L_0} m\mathbf{g}u_v\mathrm{d}s - M\mathbf{g}q_2, \tag{12}$$

where $\Pi_g^i$ is the gravitational potential energy in the undeformed reference configuration.

Hamilton's principle requires also that any virtual displacement, arbitrary between two instants $t_1$ and $t_2$, vanishes at the ends of the time interval, so that

$$\delta u_c = \delta v = \delta w = 0, \; l \leqslant s \leqslant L_1, \quad \delta u_v = 0, \; l \leqslant s \leqslant L_1, \quad \delta q_1 = \delta q_2 = 0 \tag{13a-c}$$

at $t = t_1$ and $t_2$. Inserting Eqs. (6), (8), and (12) into Eq. (5), taking into account Eq. (10) and (11), assuming that the operators $\delta$ and $\partial/\partial t$, as well as $\delta$ and $\partial/\partial s$, are commutative, and also that integration with respect to $t$ and $s$ are interchangeable, integrating by parts where necessary, both

with respect to $s$ and $t$, accounting for Eqs. (13a)–(13c), and noting that

$$\delta u_c(l,t) = \delta v(l,t) = \delta w(l,t) = 0, \quad \delta v(L_1,t) = \delta w(L_1,t) = 0,$$
$$\delta u_c(L_1,t) = \delta u_v(L_1,t) = \delta q_1, \quad \delta u_v(L_0,t) = \delta q_2, \tag{14}$$

yields the system of equations for the dynamic deflections as

$$m(u_{c,tt} - \ddot{l}) - EA[u_{c,s} + \tfrac{1}{2}(v_{,s}^2 + w_{,s}^2)]_{,s} - T_{c,s}^i = 0, \quad l < s < L_1, \tag{15}$$

$$mv_{,tt} - EA\{[u_{c,s} + \tfrac{1}{2}(v_{,s}^2 + w_{,s}^2)]v_{,s}\}_{,s} - T_c^i v_{,ss} - T_{c,s}^i v_{,s} = 0, \quad l < s < L_1, \tag{16}$$

$$mw_{,tt} - EA\{[u_{c,s} + \tfrac{1}{2}(v_{,s}^2 + w_{,s}^2)w_{,s}]\}_{,s} - T_c^i w_{,ss} - T_{c,s}^i w_{,s} = 0, \quad l < s < L_1, \tag{17}$$

$$m(u_{v,tt} - \ddot{l}) - EAu_{v,ss} - T_{v,s}^i - m\mathbf{g} = 0, \quad L_1 < s < L_0, \tag{18}$$

$$(I/R^2)[(u_{v,tt} + u_{v,sl}\dot{l})_{s=L_1} - \ddot{l}] + EA(\varepsilon_c - \varepsilon_v)_{s=L1} + (T_c^i - T_v^i)_{s=L_1} = 0, \tag{19}$$

$$M[(u_{v,tt})_{s=L_0} - \ddot{l}] + EA(u_{v,s})_{s=L_0} + (T_v^i)_{s=L_0} - Mg = 0. \tag{20}$$

In this non-linear system, Eqs. (15)–(18) describe the dynamics of the catenary and the vertical rope, Eq. (19) represents the balance of forces across the sheave, and the last Eq. (20) defines motion of the end mass.

The equations governing the reference configuration can be extracted from system (15)–(20) by setting all time derivatives and the dynamic strain components to zero resulting in the conditions

$$T_{c,s}^i = 0, \quad T_{v,s}^i + m\mathbf{g} = 0, \quad (T_c^i - T_v^i)_{s=L_1} = 0, \quad (T_v^i)_{s=L_0} - M\mathbf{g} = 0. \tag{21–24}$$

Eq. (21) indicates that the mean catenary tension is uniform over its entire length. Integrating Eq. (22) and accounting for conditions (23) and (24) allows the expression for the catenary tension to be expressed as

$$T_c^i(l) = M\mathbf{g} + m\mathbf{g}(L_0 - L_1). \tag{25}$$

Consequently, the vertical rope tension is given as

$$T_v^i(s) = M\mathbf{g} + m\mathbf{g}(L_0 - s), \quad L_1 \leqslant s \leqslant L_0. \tag{26}$$

It is possible to reduce the differential equations of motion (15)–(20). The longitudinal inertia term $m(u_{c,tt} - \ddot{l})$ can be neglected in Eq. (15) upon assuming that the catenary cable stretches in a *quasi-static* manner [34]. This simplification, applied also by Luongo et al. [35], and Watzky [36], is a consequence of the fact that the longitudinal wave speed is large, and greatly exceeds that of the lateral waves. Therefore, taking into account condition (21), Eq. (15) can be integrated once to give

$$u_{c,s} + \tfrac{1}{2}(v_{,s}^2 + w_{,s}^2) = e(t), \tag{27}$$

where $e(t)$ represents the spatially uniform catenary strain. Hence, the equations describing the lateral dynamic response of the catenary are

$$mv_{,tt} - EAe(t)v_{,ss} - T_c^i v_{,ss} = 0, \quad mw_{,tt} - EAe(t)w_{,ss} - T_c^i w_{,ss} = 0 \tag{28, 29}$$

and are defined over the spatial interval $l < s < L_1$, with $0 \leqslant t < \infty$. It is assumed at this stage that the lateral motions, both at the drum and the sheave ends, are not allowed. This results in trivial boundary conditions for $v$ and $w$ at $s = l,\ L_1$, respectively.

Treating the sheave and the end mass $M$ as additional inertial loads applied to the system, and using conditions (22–24), the dynamic model of the vertical rope subsystem is

$$\rho(s)u_{v,tt} - EAu_{v,ss} = \rho(s)\ddot{l} - M_S u_{v,st}\dot{l}\delta(s - L_1), \tag{30}$$

where $L_1^- < s < L_0^+, \quad 0 \leqslant t \leqslant \infty$, with the boundary conditions

$$EA[e(t) - u_{v,s}(L_1^-, t)] = 0, \quad EAu_{v,s}(L_0^+, t) = 0, \tag{31a, b}$$

where $M_S = I/R^2$ is the effective mass of the sheave, $e(t)$ is given by Eq. (27), $\delta$ is the Dirac delta function, $L_1^-$ denotes the point immediately to the left of $M_S$, $L_0^+$ is the point immediately to the right of $M$, and the mass distribution function $\rho(s)$ is defined as

$$\rho = m + M_S\delta(s - L_1) + M\delta(s - L_0). \tag{32}$$

Thus, in this formulation the vertical subsystem is modelled as constrained by the catenary at $s = L_1^-$, free at $s = L_0^+$, and acted upon by an inertial load due to the axial transport motion.

### 3.2. Boundary excitation

The cable cross-over motion at the drum results in additional longitudinal, in and out-of-plane lateral displacements at $s = l$, relative to the overall rigid-body translation. This results in a boundary excitation, which can be accounted for by suitable formulation of boundary conditions at $s = l$. Thus, for the longitudinal motion the boundary condition should read

$$u_c(l, t) = u_l(t), \tag{33}$$

and for the lateral motions the boundary conditions are formulated as

$$v(l, t) = v_l(t), \quad w(l, t) = w_l(t), \tag{34}$$

where $u_l(t)$, $v_l(t)$, and $w_l(t)$ are periodic functions prescribed by the geometry of the cross-over zones.

The inertial loads in the in and out-of-plane lateral directions due to the cross-over geometry can be accommodated via a suitable coordinate transformation, with the cross-over displacements being regarded as additional rigid-body translations. Since the catenary is constrained in the lateral directions at the sheave end, these translations vary from $v_l$ and $w_l$, respectively, at the drum, to zero at the sheave. Thus, the absolute displacements $v$ and $w$ can be expressed as

$$v(s, t) = \bar{v}(s, t) + v_l(1 - (s - l)/L_c), \quad w(s, t) = \bar{w}(s, t) + w_l(1 - (s - l)/L_c), \tag{35}$$

where $\bar{v}$ and $\bar{w}$ represent displacements relative to the rigid-body motions in the lateral directions. Inserting Eq. (35) into Eqs. (28) and (29), respectively, the catenary dynamics is described by

$$m\bar{v}_{,tt} - T_c^i\bar{v}_{,ss} = EAe(t)\bar{v}_{,ss} + F_v(s,t), \tag{36a}$$

$$m\bar{w}_{,tt} - T_c^i\bar{w}_{,ss} = EAe(t)\bar{w}_{,ss} + F_w(s,t), \tag{36b}$$

defined over the spatial interval $l<s<L_1^-$, with trivial boundary conditions for $\bar{v}$ and $\bar{w}$ at $s = l, L_1$, and where the inertial loads $F_v$ and $F_w$ are defined as

$$\begin{aligned} F_v(s,t) &= -m[\ddot{v}_l(1-(s-l)/L_c) + 2\dot{v}_l(\dot{l}/L_c) + v_l(\ddot{l}/L_c)], \\ F_w(s,t) &= -m[\ddot{w}_l(1-(s-l)/L_c) + 2\dot{w}_l(\dot{l}/L_c) + w_l(\ddot{l}/L_c)]. \end{aligned} \tag{37}$$

Furthermore, the catenary strain $e$ can be determined from Eq. (27). Integrating, and using the boundary condition (33) gives

$$u_c(s,t) = u_l(t) + (s-l)e(t) - \frac{1}{2}\int_l^s (v_{,s}^2 + w_{,s}^2)\mathrm{d}s. \tag{38}$$

Consequently, when the continuity of longitudinal deflection across the sheave is accounted for,

$$e(t) = \frac{1}{L_c}\left[u_v(L_1,t) - u_l(t) + \frac{1}{2}\int_l^{L_1}(v_{,s}^2 + w_{,s}^2)\mathrm{d}s\right]. \tag{39}$$

When the boundary conditions (34) are used, together with transformations (35), the catenary strain is given as

$$e(t) = \frac{1}{L_c}\left[u_v(L_1,t) - u_l + \frac{1}{2}\int_l^{L_1}(\bar{v}_{,s}^2 + \bar{w}_{,s}^2)\mathrm{d}s + \frac{1}{2L_c}(v_l^2 + w_l^2) - \frac{1}{L_c}\int_l^{L_1}(v_l\bar{v}_{,s} + w_l\bar{w}_{,s})\mathrm{d}s\right]. \tag{40}$$

This result can be accommodated in the boundary condition (31a) as

$$k_c u_v(L_1^-,t) - EAu_{v,s}(L_1^-,t) = k_c[u_l(t) - f_c(t)], \tag{41}$$

where $k_c = EA/L_c$, and

$$f_c(t) = \frac{1}{2}\int_l^{L_1}(\bar{v}_{,s}^2 + \bar{w}_{,s}^2)\mathrm{d}s + \frac{1}{2L_c}(v_l^2 + w_l^2) - \frac{1}{L_c}\int_l^{L_1}(v_l\bar{v}_{,s} + w_l\bar{w}_{,s})\mathrm{d}s. \tag{42}$$

Consequently, the dynamic model of the vertical rope is formulated as

$$\rho(s)u_{v,tt} - EAu_{v,ss} = \rho(s)\ddot{l} + \left\{k_c[u_l(t) - f_c(t)] - M_S u_{v,st}\dot{l}\right\}\delta(s - L_1) \tag{43}$$

for $L_1^- < s < L_0^+$, with the homogeneous boundary conditions

$$k_c u_v(L_1^-,t) - EAu_{v,s}(L_1^-,t) = 0, \quad EAu_{v,s}(L_0^+,t) = 0, \tag{44a, b}$$

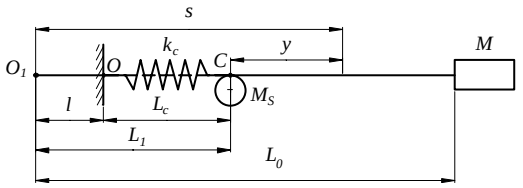


Fig. 5. The vertical (longitudinal) system.

Hence, the undamped response of the hoisting cable system is defined by Eqs. (36a) and (36b) for the catenary cable ($l<s<L_1^-$), with trivial boundary conditions, and by Eq. (43) for the vertical system ($L_1^-<s<L_0^+$), with boundary conditions (44a)–(44b). In this formulation, the vertical system, as depicted schematically in Fig. 5, is modelled as a system constrained at $s=L_1^-$ by a linear spring of constant $k_c$, representing the longitudinal elastic catenary effects, and free at $s=L_0^+$. This system is acted upon by an inertial load due to the transport motion, and is subjected to the boundary excitation and to an elastic force resulting from the catenary lateral strain.

### 3.3. Damping model

The correct definition of damping in the system presents a difficult problem, as both lateral and longitudinal damping mechanisms in hoisting steel wire cables are complex phenomena. However, it is a recognized practice to replace resisting forces of a complicated nature by equivalent viscous damping for purposes of analysis [37,38]. The equivalent damping coefficients can then be determined from energy considerations and experimentally. For example, Kumaniecka and Niziol [15] considered the combination of viscous and dry friction damping in a steel wire rope, and found the equivalent viscous damping coefficient from the equality of the energy dissipated by dry friction forces, and the energy dissipated by the equivalent viscous damping forces over one period of vibration.

The viscous damping distributed force in a continuous structural member can be given in the form

$$F_c=-\mathscr{C}[U_{,t}], \tag{45}$$

where $\mathscr{C}$ is the proportional damping operator, and $U$ denotes the displacement. Following this approach, the catenary lateral damping forces are introduced as

$$F_{cv}=-\mathscr{C}_l[\bar{v}_{,t}],\quad F_{cw}=-\mathscr{C}_l[\bar{w}_{,t}], \tag{46a, b}$$

where $\mathscr{C}_l$ denotes the lateral proportional damping operator and is defined as

$$\mathscr{C}_l=-\lambda_1 T_c^i(\partial^2/\partial s^2)+\lambda_2 m, \tag{47}$$

where $\lambda_1$ and $\lambda_2$ are constant coefficients of lateral damping. Similarly, the vertical rope damping force can be expressed as

$$F_{cu}=-\mathscr{C}_u[u_{v,t}], \tag{48}$$

where $\mathscr{C}_u$ denotes the longitudinal proportional damping operator given as

$$\mathscr{C}_u=-\mu_1 EA(\partial^2/\partial s^2)+\mu_2\rho, \tag{49}$$

where $\mu_1$ and $\mu_2$ are coefficients of longitudinal damping.

Thus, when the damping terms are taken into consideration, the response of the system is governed by

$$m\bar{v}_{,tt}-\lambda_1 T_c^i\bar{v}_{,sst}+\lambda_2 m\bar{v}_{,t}-T_c^i\bar{v}_{,ss}=EAe(t)\bar{v}_{,ss}+F_v(s,t), \tag{50}$$

$$m\bar{w}_{,tt}-\lambda_1 T_c^i\bar{w}_{,sst}+\lambda_2 m\bar{w}_{,t}-T_c^i\bar{w}_{,ss}=EAe(t)\bar{w}_{,ss}+F_w(s,t), \tag{51}$$

$$\rho u_{v,tt}-\mu_1 EAu_{v,sst}+\mu_2\rho u_{v,t}-EAu_{v,ss}=\rho\ddot{l}+\{k_c[u_l(t)-f_c(t)]-M_S u_{v,st}\dot{l}\}\delta(s-L_1), \tag{52}$$

where the lateral equations of motion (50) and (51) are defined over $l<s<L_1^-$ with trivial boundary conditions, and the longitudinal equation of motion (52) is defined over $L_1^-<s<L_0^+$ with the boundary conditions remaining in the form of Eqs. (44a) and (44b).

Thus, the equations of motion of the catenary–vertical rope system are non-linear in nature. The source of non-linearity in this system is the large displacement catenary approximation, and therefore is of geometric kind. Besides, these equations are defined over time-dependent spatial domain rendering the problem non-stationary. Hence, the exact solution to this problem is not available, and recourse must be made to an approximate analysis. In what follows, the spatial variation of displacements is assumed in terms of the linear slowly varying undamped natural modes of the system, and the Rayleigh–Ritz procedure is employed to obtain a set of non-linear, non-stationary, coupled second order ordinary differential equations describing the temporal behaviour of the system.

## 4. Discrete mathematical model

The equations of motion (50), (51) and (52) can be discretized by applying the Rayleigh–Ritz procedure. Hence, the dynamic response of the catenary (lateral) system is approximated by the expansions

$$\bar{v}=\sum_{n=1}^{N_{lat}}\Phi_n(s,l)p_n(t),\quad \bar{w}=\sum_{n=1}^{N_{lat}}\Phi_n(s,l)q_n(t), \tag{53a, b}$$

where $p_n$ and $q_n$ are generalized (modal) coordinates, and $\Phi_n$ are linear free-oscillation modes of the corresponding undamped stationary system. The in-plane and the out-of-plane modes $\Phi_n$ are assumed to be identical, and equivalent to those of a taut string, which in the co-ordinate system used are given as

$$\Phi_n=\sin[(n\pi/L_c)(s-l)]. \tag{54}$$

The corresponding natural frequencies are defined as $\bar{\omega}_n(l)=(n\pi/L_c)\bar{c}$, where $\bar{c}=\sqrt{T_c^i(l)/m}$, with the mean tension $T_c^i$ given by Eq. (25). An approximate dynamic response of the vertical (longitudinal) system is represented by the series

$$u_v=\sum_{n=1}^{N_{long}}Y_n(s,l)z_n(t), \tag{55}$$

where $z_n(t)$ are generalized co-ordinates, and the shape functions $Y_n$ are given as free-oscillation modes of the corresponding system constrained at $s=L_1^-$ by the catenary spring, with the parameter $l$ considered to be instantaneously frozen, as shown in Fig. 5. These modes are given by

$$Y_n(s,l)=\cos\gamma_n y(s,l)+((1/L_c\gamma_n)-\gamma_n(M_S/m))\sin\gamma_n y(s,l), \tag{56}$$

where $\gamma_n=\omega_n(l)/c$, with $c=\sqrt{EA/m}$, and $\omega_n$ represents the longitudinal natural frequency, and $y=s-L_1$. The eigenvalues $\gamma_n$ are determined from the frequency equation

$$\left(\frac{1}{L_c}-\frac{M_S}{m}\gamma_n^2\right)\left(\cos\gamma_n L_v-\frac{M}{m}\gamma_n\sin\gamma_n L_v\right)-\gamma_n\left(\frac{M}{m}\gamma_n\cos\gamma_n L_v+\sin\gamma_n L_v\right)=0, \tag{57}$$

where $L_v=L_0-L_1$.

Consequently, expansions (53a), (53b) and (55) result in the expressions for partial derivatives of the lateral and longitudinal displacement functions:

$$\bar{v}_{,t} = \sum_{n=1}^{L_{lat}} \left( \frac{\partial \Phi_n}{\partial l} \dot{l} p_n + \Phi_n \dot{p}_n \right), \quad \bar{w}_{,t} = \sum_{n=1}^{N_{lat}} \left( \frac{\partial \Phi_n}{\partial l} \dot{l} q_n + \Phi_n \dot{q}_n \right), \tag{58}$$

$$\bar{v}_{,s} = \sum_{n=1}^{N_{lat}} \Phi'_n p_n, \quad \bar{w}_{,s} = \sum_{n=1}^{N_{lat}} \Phi'_n q_n, \tag{59}$$

$$\bar{v}_{,tt} = \sum_{n=1}^{N_{lat}} \left[ \left( \frac{\partial^2 \Phi_n}{\partial l^2} \dot{l}^2 + \frac{\partial \Phi_n}{\partial l} \ddot{l} \right) p_n + 2 \frac{\partial \Phi_n}{\partial l} \dot{l} \dot{p}_n + \Phi_n \ddot{p}_n \right], \tag{60a}$$

$$\bar{w}_{,tt} = \sum_{n=1}^{N_{lat}} \left[ \left( \frac{\partial^2 \Phi_n}{\partial l^2} \dot{l}^2 + \frac{\partial \Phi_n}{\partial l} \ddot{l} \right) q_n + 2 \frac{\partial \Phi_n}{\partial l} \dot{l} \dot{q}_n + \Phi_n \ddot{q}_n \right], \tag{60b}$$

$$\bar{v}_{,ss} = \sum_{n=1}^{N_{lat}} \Phi''_n p_n, \quad \bar{w}_{,ss} = \sum_{n=1}^{N_{lat}} \Phi''_n q_n, \tag{61}$$

$$\bar{v}_{,st} = \sum_{n=1}^{N_{lat}} \left( \frac{\partial \Phi'_n}{\partial l} \dot{l} p_n + \Phi'_n \dot{p}_n \right), \quad \bar{w}_{,st} = \sum_{n=1}^{N_{lat}} \left( \frac{\partial \Phi'_n}{\partial l} \dot{l} q_n + \Phi'_n \dot{q}_n \right), \tag{62}$$

$$\bar{v}_{,sst} = \sum_{n=1}^{N_{lat}} \left( \frac{\partial \Phi''_n}{\partial l} \dot{l} p_n + \Phi''_n \dot{p}_n \right), \quad \bar{w}_{,sst} = \sum_{n=1}^{N_{lat}} \left( \frac{\partial \Phi''_n}{\partial l} \dot{l} q_n + \Phi''_n \dot{q}_n \right), \tag{63}$$

$$u_{v,t} = \sum_{n=1}^{N_{lat}} \left( \frac{\partial Y_n}{\partial l} \dot{l} z_n + Y_n \dot{z}_n \right), \tag{64}$$

$$u_{v,tt} = \sum_{n=1}^{N_{long}} \left[ \left( \frac{\partial^2 Y_n}{\partial l^2} \dot{l}^2 + \frac{\partial Y_n}{\partial l} \ddot{l} \right) z_n + 2 \frac{\partial Y_n}{\partial l} \dot{l} \dot{z}_n + Y_n \ddot{z}_n \right], \quad u_{v,ss} = \sum_{n=1}^{N_{long}} Y''_n z_n, \tag{65, 66}$$

$$u_{v,st} = \sum_{n=1}^{N_{long}} \left( \frac{\partial Y'_n}{\partial l} \dot{l} z_n + Y'_n \dot{z}_n \right), \quad u_{v,sst} = \sum_{n=1}^{N_{long}} \left( \frac{\partial Y''_n}{\partial l} \dot{l} z_n + Y''_n \dot{z}_n \right). \tag{67}$$

where the primes denote partial derivatives with respect to $s$. Furthermore, it can be also found from Eq. (56) that

$$Y'_n = -\gamma_n [\sin \gamma_n y - (1/(L_c \gamma_n) - (M_S/m)\gamma_n) \cos \gamma_n y], \tag{68a}$$

$$\begin{aligned} \frac{\partial Y'_n}{\partial l} = & -\left( \frac{\mathrm{d}\gamma_n}{\mathrm{d}l} y - \gamma_n \right) \left[ \gamma_n \cos \gamma_n y + \left( \frac{1}{L_c} - \frac{M_S}{m} \gamma_n^2 \right) \sin \gamma_n y \right] \\ & - \frac{\mathrm{d}\gamma_n}{\mathrm{d}l} \left[ \sin \gamma_n + 2 \frac{M_S}{m} \gamma_n \cos \gamma_n y \right], \end{aligned} \tag{68b}$$

so that

$$Y'(L_1,l)=\gamma_n(1/(L_c\gamma_n)-(M_S/m)\gamma_n),\quad (\partial Y'_n/\partial l)(L_1,l)=\gamma_n^2-2(M_S/m)\gamma_n(\mathrm{d}\gamma_n/\mathrm{d}l). \tag{69a, b}$$

By substituting series (59) into the expression (40) the discretized form of the catenary strain $e$ can be obtained. This is accomplished by finding directly from expansions (53a) and (53b) that

$$\bar{v}_{,s}^2=\sum_{i=1}^{N_{lat}}\sum_{j=1}^{N_{lat}}p_ip_j\Phi'_i\Phi'_j,\quad \bar{w}_{,s}^2=\sum_{i=1}^{N_{lat}}\sum_{j=1}^{N_{lat}}q_iq_j\Phi'_i\Phi'_j, \tag{70a, b}$$

so that, when the orthogonality properties of the lateral modes are applied,

$$\int_l^{L_1}(\bar{v}_{,s}^2+\bar{w}_{,s}^2)\mathrm{d}s=\frac{\pi^2}{2L_c}\sum_{n=1}^{N_{lat}}n^2(p_n^2+q_n^2). \tag{71}$$

Noting also that

$$\int_l^{L_1}\bar{v}_{,s}=\int_l^{L_1}\bar{w}_{,s}=0, \tag{72}$$

and applying series (55) with eigenfunctions (56) to express the deflection at the sheave as $u_v(L_1,t)=\sum_{n=1}^{N_{long}}z_n$, the expression for the catenary strain results is

$$e(t)=F_l(t)+\frac{1}{L_c}\sum_{n=1}^{N_{long}}z_n+\sum_{n=1}^{N_{lat}}\beta_n^2(p_n^2+q_n^2), \tag{73}$$

where $F_l(t)=(1/L_c)\{(1/(2L_c))[v_l^2(t)+w_l^2(t)]-u_l(t)\}$ and $\beta_n=n\pi/2L_c$.

By substituting expansions (58)–(63) together with the strain given by Eq. (73) into the differential equations of motion (50) and (51), and by applying the Rayleigh–Ritz procedure, the discretized lateral equations are obtained as

$$\begin{aligned}\ddot{p}_k&+2\bar{\zeta}_k\bar{\omega}_k\dot{p}_k+\bar{\omega}_k^2\left[1+\left(\frac{c}{c}\right)^2F_l(t)\right]p_k=-\frac{2}{m_k}\dot{l}\sum_{n=1}^{N_{lat}}C_{kn}\dot{p}_n\\&-\frac{1}{m_k}\sum_{n=1}^{N_{lat}}(\ddot{l}^2D_{kn}+\ddot{l}C_{kn}-\lambda_1\dot{l}T_c^iB_{kn}+\lambda_2\dot{l}C_{kn})p_n\\&-\left(\frac{c}{c}\right)^2\bar{\omega}_k^2\left[\frac{1}{L_c}\sum_{n=1}^{N_{long}}z_n+\sum_{n=1}^{N_{lat}}\beta_n^2(p_n^2+q_n^2)\right]p_k+P_k(t),\end{aligned} \tag{74}$$

$$\begin{aligned}\ddot{q}_k&+2\bar{\zeta}_k\bar{\omega}_k\dot{q}_k+\bar{\omega}_k^2\left[1+\left(\frac{c}{c}\right)^2F_l(t)\right]q_k=-\frac{2}{m_k}\dot{l}\sum_{n=1}^{N_{lat}}C_{kn}\dot{q}_n\\&-\frac{1}{m_k}\sum_{n=1}^{N_{lat}}(\ddot{l}^2D_{kn}+\ddot{l}C_{kn}-\lambda_1\dot{l}T_c^iB_{kn}+\lambda_2\dot{l}C_{kn})q_n\\&-\left(\frac{c}{c}\right)^2\bar{\omega}_k^2\left[\frac{1}{L_c}\sum_{n=1}^{N_{long}}z_n+\sum_{n=1}^{N_{lat}}\beta_n^2(p_n^2+q_n^2)\right]q_k+Q_k(t),\end{aligned} \tag{75}$$

where $k = 1, 2, \cdots, N_{lat}$, and

$$\bar{\zeta}_k = \tfrac{1}{2}\left(\lambda_1 \bar{\omega}_k + \frac{\lambda_2}{\bar{w}_k}\right), \quad m_k = m \int_l^{L_1} \Phi_k^2 \mathrm{d}s, \tag{76a, b}$$

$$B_{kn} = \int_l^{L_1} \Phi_k \frac{\partial \Phi_n''}{\partial l} \mathrm{d}s, \quad C_{kn} = m \int_l^{L_1} \Phi_k \frac{\partial \Phi_n}{\partial l} \mathrm{d}s, \quad D_{kn} = m \int_l^{L_1} \Phi_k \frac{\partial^2 \Phi_n}{\partial l^2} \mathrm{d}s, \tag{76c-e}$$

$$P_k = \frac{1}{m_k} \int_l^{L_1} \Phi_k F_v(s,t) \mathrm{d}s, \quad Q_k = \frac{1}{m_k} \int_l^{L_1} \Phi_k F_w(s,t) \mathrm{d}s. \tag{76f, g}$$

Similarly, the non-linear longitudinal equation of motion (52) is discretized by using the expansion (55) together with (53a) and (53b). Noting that this transforms Eq. (42) into the form

$$f_c(t) = \frac{1}{2L_c}\left[\sum_{n=1}^{N_{lat}} \frac{n^2\pi^2}{2}(p_n^2 + q_n^2) + v_l^2 + w_l^2\right], \tag{77}$$

the Rayleigh–Ritz method yields

$$\begin{aligned} \ddot{z}_r + \mu_2 \dot{z}_r + \omega_r^2 z_r \; = & \frac{1}{m_r^v} \sum_{n=1}^{N_{long}} \left[2\dot{l} C_{rn}^v - EA\Lambda_{rn} + M_S \dot{l}\left(\frac{1}{L_c} - \frac{M_s}{m}\gamma_n^2\right)\right] \dot{z}_n \\ & - \frac{1}{m_r^v} \sum_{n=1}^{N_{long}} (\dot{l}^2 D_{rn}^v + \ddot{l} C_{rn}^v - EA\dot{l} B_{rn}^v + \mu_2 \dot{l} C_{rn}^v + M_S \dot{l}^2 \Gamma_n) z_n \\ & - \frac{EA}{m_r^v}\left[\sum_{n=1}^{N_{lat}} \beta_n^2 (p_n^2 + q_n^2) + F_l(t)\right] + Z_r, \end{aligned} \tag{78}$$

where $r = 1, 2, \cdots, N_{long}$, and the non-stationary coefficients $m_r^v$, $B_{rn}^v$, $C_{rn}^v$, $D_{rn}^v$, $\Gamma_n$, $\Lambda_{rn}$, and the excitation term $Z_r$ are defined as

$$m_r^v = \int_{L_1}^{L_0} \rho(s) Y_r^2 \mathrm{d}s, \quad B_{rn}^v = \int_{L_1}^{L_0} \mu_1 Y_r \frac{\partial Y_n''}{\partial l} \mathrm{d}s, \tag{79a, b}$$

$$C_{rn}^v = \int_{L_1}^{L_0} \rho(s) Y_r \frac{\partial Y_n}{\partial l} \mathrm{d}s, \quad D_{rn}^v = \int_{L_1}^{L_0} \rho(s) Y_r \frac{\partial^2 Y_n}{\partial l^2} \mathrm{d}s, \tag{79c, d}$$

$$\Gamma_n = \gamma_n\left(\gamma_n - 2\frac{M_S}{m}\frac{\mathrm{d}\gamma_n}{\mathrm{d}l}\right), \quad \Lambda_{rn} = \int_{L_1}^{L_0} \mu_1 Y_r Y_n'' \mathrm{d}s, \quad Z_r = \frac{\ddot{l}}{m_r^v} \int_{L_1}^{L_0} \rho(s) Y_r \mathrm{d}s. \tag{79e-g}$$

It should be noted that the lateral coefficients and excitation terms (76b)–(76g) can be determined directly, and are given as

$$m_k = \tfrac{1}{2} m L_c, \quad B_{kn} = \left\{ \begin{array}{l} -(\frac{\pi}{L_c})^2 \, \frac{kn^3[(-1)^{k+n}-1]}{k^2-n^2}, \; k \neq n. \\ 0, \; k = n, \end{array} \right\}, \tag{80a, b}$$

$$C_{kn} = \left\{ \begin{array}{l} m\frac{kn[(-1)^{k+n}-1}{k^2-n^2}, \; k \neq n \\ 0, \; k = n \end{array} \right\}, \quad D_{kn} = \left\{ \begin{array}{l} 0, \; k \neq n \\ -m\frac{n^2\pi}{2L_c}, \; k = n \end{array} \right\}, \tag{80c, d}$$

$$P_k = -\frac{2}{k\pi}\left\{\ddot{v}_l - \left(2\dot{v}_l\frac{\dot{l}}{L_c} + v_l\frac{\ddot{l}}{L_c}\right)[(-1)^k - 1]\right\},$$
$$Q_k = -\frac{2}{k\pi}\left\{\ddot{w}_l - \left(2\dot{w}_l\frac{\dot{l}}{L_c} + w_l\frac{\ddot{l}}{L_c}\right)[(-1)^k - 1]\right\}. \quad (80e, f)$$

However, the longitudinal coefficients and excitation terms appearing in the longitudinal equation (78) depend on the non-stationary eigenvalues $\gamma_n$, and must be calculated numerically following the procedure outlined in the appendix.

It should be noted that the lateral natural frequency in Eqs. (74) and (75), as well as the longitudinal natural frequency and coefficients in Eq. (78) depend on the non-stationary parameter $l$, and are varying slowly. Hence, their variation can be observed on a slow time scale defined as $\tau = \varepsilon T$, where $\varepsilon$ is a small parameter. This parameter can be defined in terms of the winding velocity, so that it is directly related to the rate of change of the vertical rope length [39]. Moreover, $T$ denotes the fast scale given as $T = \omega_0 t$, where $\omega_0$ is the initial fundamental frequency of the entire system. Consequently, a variation of the generalized co-ordinates $p_k$, $q_k$, and $z_r$ are observed on the fast scale. By assuming that the damping is small, the lateral and longitudinal damping coefficients are ordered as

$$\lambda_i = \varepsilon\lambda_i^*, \quad \mu_i = \varepsilon\mu_i^*, \quad (81, 82)$$

where $i = 1,2$. Consequently, the lateral damping ratios are given as

$$\bar{\zeta}_k = \varepsilon\bar{\zeta}_k^*, \quad k = 1, 2, \cdots, N_{lat} \quad (83)$$

Therefore, by noting that $\dot{l} = \omega_0\varepsilon(\mathrm{d}l/\mathrm{d}\tau)$, $\ddot{l} = \omega_0^2\varepsilon^2(\mathrm{d}^2l/\mathrm{d}\tau^2)$, and by substituting the time derivatives of the in- and out-of-plane, and longitudinal temporal co-ordinates given as

$$\dot{p}_k = \omega_0\frac{\mathrm{d}p_k}{\mathrm{d}T}, \quad \ddot{p}_k = \omega_0^2\frac{\mathrm{d}^2p_k}{\mathrm{d}T^2}, \quad (84)$$

$$\dot{q}_k = \omega_0\frac{\mathrm{d}q_k}{\mathrm{d}T}, \quad \ddot{q}_k = \omega_0^2\frac{\mathrm{d}^2q_k}{\mathrm{d}T^2}; \quad \dot{z}_r = \omega_0\frac{\mathrm{d}z_r}{\mathrm{d}T}, \quad \ddot{z}_r = \omega_0^2\frac{\mathrm{d}^2z_r}{\mathrm{d}T^2} \quad (85, 86)$$

for $k = 1, 2, \cdots, N_{lat}$, $r = 1, 2, \cdots, N_{long}$ respectively, into Eqs. (74), (75), and (78), results in:

$$\frac{\mathrm{d}^2p_k}{\mathrm{d}T^2} + \hat{\omega}_k^2(\tau)\left[1 + \left(\frac{c}{\bar{c}}\right)^2 F_l(T)\right]p_k = \varepsilon f_k^p\left(\tau, \frac{\mathrm{d}p_1}{\mathrm{d}T}, \cdots, \frac{\mathrm{d}p_{N_{lat}}}{\mathrm{d}T}\right)$$
$$- \left(\frac{c}{\bar{c}}\right)^2\hat{\omega}_k^2(\tau)\left[\frac{1}{L_c}\sum_{n=1}^{N_{long}} z_n + \sum_{n=1}^{N_{long}}\beta_n^2(p_n^2 + q_n^2)\right]p_k + \hat{P}_k(\tau, T) + O(\varepsilon^2), \quad (87)$$

$$\frac{\mathrm{d}^2q_k}{dT^2} + \hat{\omega}_k^2(\tau)\left[1 + \left(\frac{c}{\bar{c}}\right)^2 F_l(T)\right]q_k = \varepsilon f_k^q\left(\tau, \frac{\mathrm{d}q_1}{\mathrm{d}T}, \cdots, \frac{\mathrm{d}q_{N_{lat}}}{\mathrm{d}T}\right)$$
$$-\left(\frac{c}{\bar{c}}\right)^2\hat{\omega}_k^2(\tau)\left[\frac{1}{L_c}\sum_{n=1}^{N_{long}} z_n + \sum_{n=1}^{N_{long}}\beta_n^2(p_n^2 + q_n^2)\right]q_k + \hat{Q}_k(\tau, T) + O(\varepsilon^2), \quad (88)$$

where $k = 1, 2, \cdots, N_{lat}, \hat{\omega}_k = \dfrac{\bar{\omega}_k}{\hat{\omega}_0}, \hat{P}_k = \dfrac{P_k}{\omega_0^2}, \hat{Q}_k = \dfrac{Q_k}{\omega_0^2}$ and

$$\frac{\mathrm{d}^2 z_r}{\mathrm{d}T^2} + \tilde{\omega}_r^2(\tau) z_r = \varepsilon f_r^z \left(\tau, \frac{\mathrm{d}z_1}{\mathrm{d}T}, \cdots, \frac{\mathrm{d}z_{N_{long}}}{\mathrm{d}T}\right) - \frac{EA}{\omega_0^2 m_r^v(\tau)} \left[\sum_{n=1}^{N_{lat}} \beta_n^2 (p_n^2 + q_n^2) + F_l(T)\right] + \hat{Z}_r(\tau, T) + O(\varepsilon^2), \tag{89}$$

where $r = 1, 2, \cdots, N_{long}, \tilde{\omega}_r = \omega_r/\omega_0, \hat{Z}_r = Z_r/\omega_0^2$ and

$$f_k^p = -2\left[\frac{1}{m_k}\frac{\mathrm{d}l}{\mathrm{d}\tau}\sum_{n=1}^{N_{lat}} C_{kn}\frac{\mathrm{d}p_n}{\mathrm{d}T} + \bar{\zeta}_k^* \hat{\omega}_k \frac{\mathrm{d}p_k}{\mathrm{d}T}\right], \quad f_k^q = -2\left[\frac{1}{m_k}\frac{\mathrm{d}l}{\mathrm{d}\tau}\sum_{n=1}^{N_{lat}} C_{kn}\frac{\mathrm{d}q_n}{\mathrm{d}T} + \bar{\zeta}_k^* \hat{\omega}_k \frac{\mathrm{d}q_k}{\mathrm{d}T}\right], \tag{90a, b}$$

$$f_r^z = -\frac{1}{m_r^v(\tau)}\sum_{n=1}^{N_{long}}\left[2\frac{\mathrm{d}l}{\mathrm{d}\tau}C_{rn}^v(\tau) - \frac{EA}{\omega_0}\Lambda_{rn}^* + M_S\frac{\mathrm{d}l}{\mathrm{d}\tau}\left(\frac{1}{L_c} - \frac{M_S}{m}\gamma_n^2\right)\right]\frac{\mathrm{d}z_n}{\mathrm{d}T} - \frac{\mu_2^*}{\omega_0}\frac{\mathrm{d}z_r}{\mathrm{d}T}, \tag{90c}$$

where $\Lambda_{rn}^*(\tau) = \int_{L_1}^{L_0} \mu_1^* Y_r Y_n'' \mathrm{d}s$.

The discrete model equations (87)–(89) form a non-linear slowly varying ordinary differential equation system. It describes the interactions between lateral oscillations of the catenary cable and longitudinal oscillations of the vertical rope in the hoisting cable system. In the catenary (lateral) system, a quadratic coupling between the lateral and the longitudinal modes exists, and a cubic coupling arises between the in- and out-of-plane lateral modes. In the vertical rope (longitudinal), system a quadratic coupling with the lateral modes results. The lateral and longitudinal natural frequencies change with time, and linear coupling terms due to the non-stationary nature of the natural modes arise. The lateral system equations contain parametric excitation terms. Terms representing the inertial load due to the axial transport motion, and the cross-over external excitation are present in both systems.

## 5. Prediction of resonance and modal interaction phenomena

The mathematical model defined by Eqs. (87)–(89) illustrates the true dynamic nature of the catenary–vertical rope system, and can be used to predict and analyze important resonance phenomena that arise when certain frequency tuning conditions take place. These phenomena may include external, parametric and autoparametric (internal) resonances, as well as non-linear modal interactions and an energy exchange among the modes.

Consider an ascending cycle of a typical deep mine system with the fundamental parameters given in Table 1. Both the longitudinal and lateral natural frequencies of the system vary slowly during this cycle, as shown in Fig. 6. The first four longitudinal and lateral natural frequencies of the system, and the first and the second harmonics of the excitation frequencies corresponding to winding velocities $V_c$ = 14, 15, 16, and 19.5 m/s, given as

$$\Omega_n = 2n(V_c/R_d), \quad n = 1, 2, \tag{91}$$

Table 1
Kloof system parameters

| | |
|---|---|
| Total winding cycle time (s) | 156 |
| Acceleration/deceleration time (s) | 19.7 |
| Nominal hoisting velocity $V_c$ (m/s) | 15 |
| Total hoisted mass $M$ (kg) | 17 584 |
| Sheave wheel moment of inertia $I$ (kgm$^2$) | 15 200 |
| Winder drum radius $R_d$ (m) | 2.14 |
| Sheave wheel radius $R$ (m) | 2.13 |
| Cable diameter $d$ (m) | $48 \times 10^{-3}$ |
| Cable linear density $m$ (kg/m) | 8.4 |
| Cable effective steel area $A$ (m$^2$) | $1.028 \times 10^{-3}$ |
| Cable effective Young's Modulus $E$ (N/m$^2$) | $1.1 \times 1011$ |
| Catenary length $L_c$ (m) | 74.95 |
| Maximum depth of winding $L_{v\ max}$ (m) | 2100 |

are shown in this figure versus the vertical rope length. The longitudinal frequencies increase, and the lateral frequencies decrease, with the decreasing length of the rope. It should be noted that the natural modes are widely spaced with the largest spread between the longitudinal and the lateral natural frequencies taking place at the end of the wind when the third and fourth longitudinal frequencies (curves labelled as $3_{long}$ and $4_{long}$, respectively) become very high. Thus, the problem is numerically *stiff*, and in order to solve Eqs. (87)–(89) the application of special algorithms would be required.

Taking into consideration the quadratic coupling between the longitudinal and lateral modes, and the cubic coupling between the in- and out-of-plane lateral modes, a number of resonance conditions arise during the wind. One-to-one (1:1) lateral internal resonances occur throughout the wind since the in- and out-of-plane lateral natural frequencies are the same. Upon close examination of the frequency chart given in Fig. 6, one can notice that interesting frequency tunings occur in the depth region $L_v = 900$–$700$ m At the depth $L_v \approx 900$ m the fourth longitudinal and the second lateral natural frequencies are in the ratio 2:1, and a two-to-one ($\omega_4 \approx 2\bar{\omega}_2$) internal resonance condition takes place. At the nominal winding velocity of $V_c = 15$ m/s a primary external resonance exists simultaneously with this condition, since at this level the second harmonic of the cross-over motion $\Omega_2 = 28.04$ rad/s directly excites the fourth longitudinal mode ($\Omega_2 = \omega_4$).

Furthermore, at the depth $L_v \approx 750$m the second longitudinal frequency is near twice that of the first lateral natural frequency ($\omega_2 \approx 2\bar{\omega}_1$), so that another two-to-one internal resonance arises. At the same time, the second longitudinal frequency is tuned closely to the second lateral frequency ($\omega_2 \approx \bar{\omega}_2$), implicating also a one-to-one internal resonance. At the nominal winding speed, at this depth the model is also involved in primary external resonances, since the first harmonic of the cross-over excitation ($\Omega_1 = 14.02$) rad/s is near the second longitudinal natural frequency and the second lateral frequency ($\Omega_1 \approx \omega_2 = \bar{\omega}_2$), and also the second harmonic of the excitation is near the fourth lateral natural frequency ($\Omega_2 \approx \bar{\omega}_4$). Principal parametric resonances of the first and the second lateral modes occur at the same time, namely the resonances $\Omega_1 \approx 2\bar{\omega}_1$ and $\Omega_2 \approx 2\bar{\omega}_2$, and also the summed combination resonance $\Omega_2 \approx \omega_2 + \bar{\omega}_2$ exists. In addition to these conditions, the primary resonances $\Omega_1 \approx \omega_3$ at $L_v \approx 1500$ m, and $\Omega_2 \approx \omega_3$ at $L_v \approx 500$ m occur during the wind.

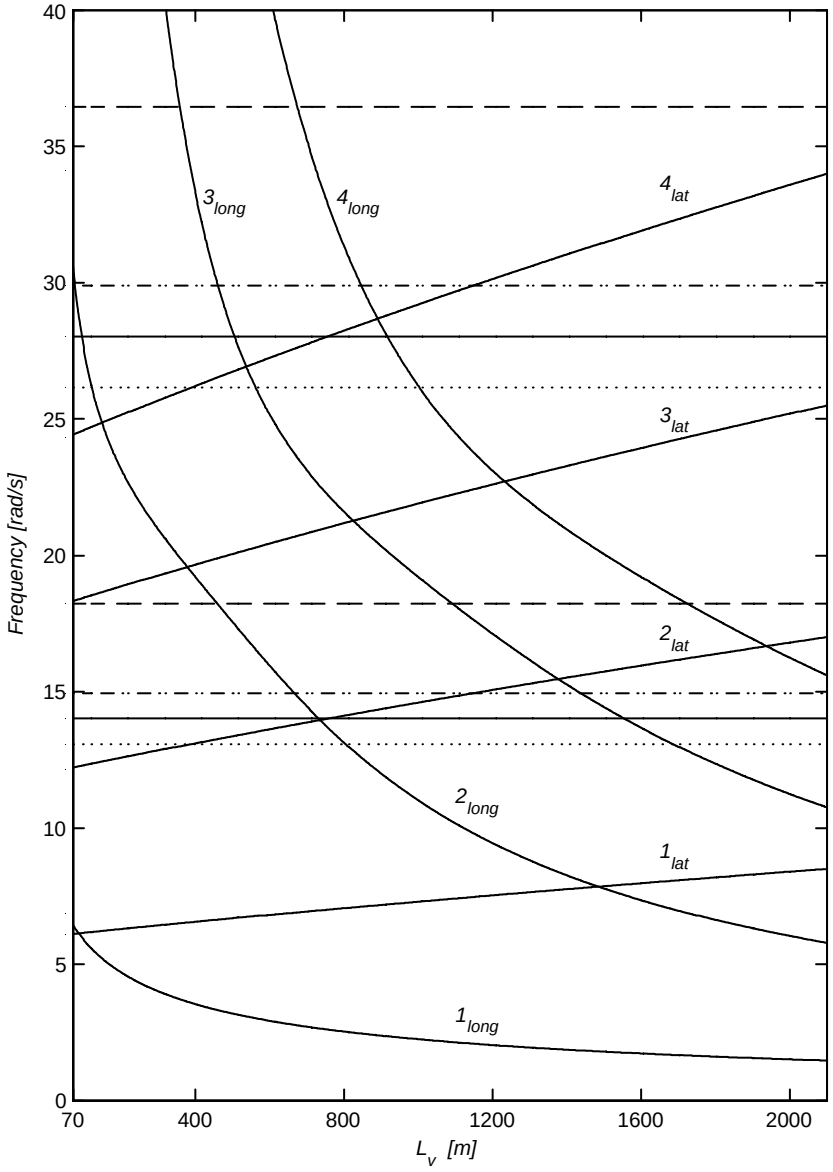


Fig. 6. The longitudinal frequency $\omega_n$ (curved solid lines, $n_{long}$) and lateral frequency $\bar{\omega}_n$ (inclined solid lines, $n_{lat}$) plot for Kloof Gold Mine winder (ascending cycle). The horizontal lines denote the first and the second harmonics of the excitation frequency: at the nominal winding velocity $V_c = 15$ m/s, (—)and at $V_c = 14(\ldots)$, 16 $(-\cdot\cdot-)$ and 19.5$(--)$m/s, respectively.

When the winding velocity is changed some resonance locations are shifted. This is due to the fact that the frequencies of excitation depend directly on this velocity, as shown in Eq. (91). For example, when the winding velocity is decreased to 14 m/s the first and second harmonics of the cross-over excitation are $\Omega_1 = 13.08$ rad/s and $\Omega_2 = 26.16$ rad/s, respectively. Consequently, at the depth $L_v = 400$ m the second lateral mode is tuned to the fundamental harmonic of the

excitation, and simultaneously the fourth lateral mode is tuned to the second harmonic of the excitation. Hence, the primary resonances $\Omega_1 \approx \bar{\omega}_2$ and $\Omega_2 \approx \bar{\omega}_4$ take place. Since the second lateral natural frequency is twice the first lateral natural frequency ($\bar{\omega}_2 = 2\bar{\omega}_1$), and the fourth lateral natural frequency is twice the second lateral natural frequency ($\bar{\omega}_4 = 2\bar{\omega}_2$), the catenary cable is simultaneously involved in the principal parametric resonances $\Omega_1 \approx 2\bar{\omega}_1$ and $\Omega_2 \approx 2\bar{\omega}_2$. Besides, passages through longitudinal primary resonances occur during the wind. In particular, the third longitudinal mode is directly activated by the fundamental harmonic of the excitation ($\Omega_1 \approx \omega_3$) at the depth level $L_v \approx 1700$ m, and later by the second harmonic of the excitation ($\Omega_2 \approx \omega_3$) at $L_v \approx 550$m. Also, at $L_v \approx 1000$ m the fourth longitudinal mode tunes to the second harmonic of the excitation ($\Omega_2 \approx \omega_4$), and at $L_v \approx 800$ m the second longitudinal mode tunes to the fundamental harmonic of the excitation ($\Omega_1 \approx \omega_2$). When the winding velocity is increased to 16 m/s, the first two harmonics of the cross-over excitation are $\Omega_1 = 14.95$ rad/s and $\Omega_2 = 29.9$ rad/s, respectively, and consequently the primary and parametric catenary resonances are shifted towards the halfway depth level, and occur at $L_v \approx 1150$ m. The catenary resonance can be avoided throughout the main part of the ascending cycle if the winding velocity is further raised. This is illustrated in Fig. 6 for a velocity of 19.5 m/s. However, as one can notice, it is not possible to evade the longitudinal resonances within the winding cycle, and autoparametric interactions between the in- and out-of-plane lateral modes will occur throughout the wind despite the winding velocity modifications.

## 6. Conclusions

A typical deep mine hoisting cable installation has been modelled as a distributed-parameter system with discrete inertial elements, resulting in the catenary–vertical rope model. Consequently, the partial differential equations of motion of this system have been derived. The large displacement catenary approximation has been used so that the non-linear coupling between the lateral and longitudinal oscillation modes are accounted for in the mathematical model. The lateral and longitudinal natural frequencies change during the wind due to the time-varying length of the vertical rope, rendering the system non-stationary. The type of non-linearity of the system is revealed when the Rayleigh–Ritz procedure is used to formulate the discrete model. This leads to a system of slowly varying ordinary-differential equations with quadratic and cubic non-linear terms.

The response of the catenary–vertical rope system may feature a number of resonance phenomena. These phenomena include external, parametric and autoparametric resonances, and the parameters of a typical deep mine winder have been used to demonstrate the depth locations of the resonance regions during the ascending cycles with various winding velocities. It has been shown that when the winding velocity is changed the resonance locations are shifted. Consequently, the catenary resonances can be avoided, to a large extent, if the winding velocity is increased, or decreased, to an appropriate level. Still, despite this winding strategy, the longitudinal primary resonances and autoparametric interactions between the in- and out-of-plane lateral modes will take place during the wind.

This can be confirmed by solving the equations of motion. It has been demonstrated that the natural modes of the hoisting system are widely spaced, so that the problem is numerically *stiff*.

This stiff nature of the system means that the complete solution to the problem will consist of slow and fast components. Thus, an appropriate solution strategy would have to be used in order to determine the system response during the winding cycle. It is evident that due to their complexity, the equations of motion cannot be solved exactly. Therefore, an approximate solution would have to be sought in order to predict the time response levels during the wind. Consequently, a numerical analysis with efficient stiff integration algorithms will have to be employed to simulate the dynamic behaviour of the system and to achieve stable results. This analysis is presented in the subsequent article Part 2.

**Acknowledgements**

The support received from the University of Natal Research Fund is gratefully acknowledged.

## Appendix A

The coefficients and excitation terms appearing in system (78) depend on the non-stationary parameter $l$, and are defined by Eqs. (79a)–(79g) in terms of the eigenvalues $\gamma_n$, the eigenfunctions $Y_n$, and their derivatives. The eigenvalues $\gamma_n$ are found from the transcendental frequency Eq. (57) which is solved using the modified *regula falsi* method. The partial derivatives of $Y_n$ with respect to $l$ are given as

$$\frac{\partial Y_n}{\partial l} = \left(\frac{\mathrm{d}\gamma_n}{\mathrm{d}l}y - \gamma_n\right)\left[\left(\frac{1}{L_c\gamma_n} - \gamma_n\frac{M_S}{m}\right)\cos\gamma_n y - \sin\gamma_n y\right] - \left(\frac{1}{L_c\gamma_n^2} + \frac{M_S}{m}\right)\frac{\mathrm{d}\gamma_n}{\mathrm{d}l}\sin\gamma_n y, \tag{A.1}$$

$$\begin{aligned}\frac{\partial^2 Y_n}{\partial l^2} = {} & \left(2\frac{\partial\gamma_n}{\partial l} - \frac{\mathrm{d}^2\gamma_n}{\mathrm{d}l^2}y\right)\left\{\frac{\mathrm{d}\gamma_n}{\mathrm{d}l}\left(\frac{1}{L_c\gamma_n^2} + \frac{M_S}{m}\right)\cos\gamma_n y\right. \\ & \left. - \left(\frac{\mathrm{d}\gamma_n}{\mathrm{d}l}y - \gamma_n\right)\left[\left(\frac{1}{L_c\gamma_n} - \gamma_n\frac{M_S}{m}\right)\sin\gamma_n y + \cos\gamma_n y\right]\right\} \\ & - \left\{\left[\left(\frac{1}{L_c\gamma_n^2} + \frac{M_S}{m}\right)\frac{\mathrm{d}^2\gamma_n}{\mathrm{d}l^2} - \frac{2}{L_c\gamma_n^3}\left(\frac{\mathrm{d}\gamma_n}{\mathrm{d}l}\right)^2\right]\sin\gamma_n y\right. \\ & \left. + \left(\frac{\mathrm{d}\gamma_n}{\mathrm{d}l} - \gamma_n\right)\left(\frac{1}{L_c\gamma_n^2} + \frac{M_S}{m}\right)\frac{\mathrm{d}\gamma_n}{\mathrm{d}l}\cos\gamma_n y\right\}.\end{aligned} \tag{A.2}$$

The derivatives of the eigenvalues $\gamma_n$ with respect to $l$ are obtained through differentiation of the frequency Eq. (57), and are calculated as

$$\mathrm{d}\gamma_n/\mathrm{d}l = N_n(l)/D_n(l), \quad \mathrm{d}^2\gamma_n/\mathrm{d}l^2 = (1/D_n^2)((\mathrm{d}N_n/\mathrm{d}l)D_n - N_n(\mathrm{d}D_n/\mathrm{d}l)), \tag{A.3, A.4}$$

where

$$N_n = \gamma_n\left\{\left[\frac{1}{L_c} - (M_S + M)\frac{\gamma_n^2}{m}\right]\sin\gamma_n L_v + \gamma_n\left[\left(\frac{1}{L_c} - \frac{M_S}{m}\gamma_n^2\right)\frac{M}{m} + 1\right]\cos\gamma_n L_v\right\}, \tag{A.5}$$

$$\begin{aligned} D_n = {} & \left[\frac{1}{L_c}\left(L_v + \frac{M}{m}\right) - 3\frac{M_S M}{m^2}\gamma_n^2 - (M_S + M)\frac{\gamma_n^2}{m}L_v + 1\right]\sin\gamma_n L_v \\ & + \left\{2(M_S + M)\frac{\gamma_n}{m} + \left[\left(\frac{1}{L_c} - \frac{M_S}{m}\gamma_n^2\right)\frac{M}{m} + 1\right]\gamma_n L_v\right\}\cos\gamma_n L_v, \end{aligned} \tag{A.6}$$

$$\begin{aligned} \frac{\mathrm{d}N_n}{\mathrm{d}l} = {} & \frac{\mathrm{d}\gamma_n}{\mathrm{d}l}\left\{\left[\frac{1}{L_c} - (M_S + M)\frac{\gamma_n^2}{m}\right]\sin\gamma_n L_v + \gamma_n\left[\left(\frac{1}{L_c} - \frac{M_S}{m}\gamma_n^2\right)\frac{M}{m} + 1\right]\cos\gamma_n L_v\right\} \\ & + \gamma_n\left\{\left[\frac{1}{L_c} - (M_S + M)\frac{\gamma_n^2}{m}\right]\left(\frac{\mathrm{d}\gamma_n}{\mathrm{d}l}L_v - \gamma_n\right)\cos\gamma_n L_v\right. \\ & - 2\frac{M_S + M}{m}\gamma_n\frac{\mathrm{d}\gamma_n}{\mathrm{d}l}\sin\gamma_n L_v + \frac{\mathrm{d}\gamma_n}{\mathrm{d}l}\left[\left(\frac{1}{L_c} - \frac{M_S}{m}\gamma_n^2\right)\frac{M}{m} + 1\right]\cos\gamma_n L_v \\ & \left. - \gamma_n\left\{\left[2\frac{M_S M}{m^2}\gamma_n\frac{\mathrm{d}\gamma_n}{\mathrm{d}l}\cos\gamma_n L_v + \left(\frac{1}{L_c} - \frac{M_S}{m}\gamma_n^2\right)\frac{M}{m} + 1\right]\left(\frac{\mathrm{d}\gamma_n}{\mathrm{d}l}L_v - \gamma_n\right)\sin\gamma_n L_v\right\}\right\}, \end{aligned} \tag{A.7}$$

and

$$\begin{aligned} \frac{\mathrm{d}D_n}{\mathrm{d}l} = {} & -\left[6\frac{M_S M}{m^2}\gamma_n\frac{\mathrm{d}\gamma_n}{\mathrm{d}l} + \frac{1}{L_c} + \frac{M_S + M}{m}\gamma_n\left(2\frac{\mathrm{d}\gamma_n}{\mathrm{d}l}L_v - \gamma_n\right)\right]\sin\gamma_n L_v \\ & + \left[\frac{1}{L_c}\left(L_v + \frac{M}{m}\right) - 3\frac{M_S M}{m^2}\gamma_n^2 - \frac{M_S + M}{m}\gamma_n^2 L_v + 1\right]\left(\frac{\mathrm{d}\gamma_n}{\mathrm{d}l}L_v - \gamma_n\right)\cos\gamma_n L_v \\ & + \left\{\frac{2}{m}\frac{\mathrm{d}\gamma_n}{\mathrm{d}l}\left(M_S + M - \frac{M_S M}{m}\gamma_n^2 L_v\right)\right. \\ & \left. + \left[\left(\frac{1}{L_c} - \frac{M_S}{m}\gamma_n^2\right)\frac{M}{m} + 1\right]\left(\frac{\mathrm{d}\gamma_n}{\mathrm{d}l}L_v - \gamma_n\right)\right\}\cos\gamma_n L_v \\ & - \left\{2\frac{M_S + M}{m}\gamma_n + \left[\left(\frac{1}{L_c} - \frac{M_S}{m}\gamma_n^2\right)\frac{M}{m} + 1\right]\gamma_n L_v\right\}\left(\frac{\mathrm{d}\gamma_n}{\mathrm{d}l}L_v - \gamma_n\right)\sin\gamma_n L_v. \end{aligned} \tag{A.8}$$

Subsequently, noting that

$$Y_n'' = -\gamma_n^2 Y_n, \quad \partial Y_n''/\partial l = -\gamma_n(2(\mathrm{d}\gamma_n/\mathrm{d}l)\,Y_n + \gamma_n(\partial Y_n/\partial l)), \tag{A.9, A.10}$$

expressions (79a)–(79 g) are evaluated numerically.

## References

[1] H.M. Irvine, Cable Structures, MIT Press, Cambridge, MA, 1981.
[2] J.A. Vaughan, An investigation regarding the effect of kinetic shocks on winding ropes in vertical shafts, The South African Association of Engineers, Minutes of Proceedings, General Meeting, March 30th, 1904, pp. 217–245.
[3] J. Perry, Winding ropes in mines, Philosophical Magazine 11 (1906) 107–117.

[4] J.F. Perry, D.M. Smith, Mechanical breaking and its influence on winding equipment, Proceedings of the Institution of Mechanical Engineers 123 (1932) 537–620.
[5] P.J. Pollock, G.W. Alexander, Dynamic stresses in wire ropes for use on vertical shafts, Wire Ropes in Mines 12 (1950) 445–462.
[6] O.A. Goroshko, G.N. Savin, The Dynamics of Threads with Variable Length. Applications in Mine Hoist Systems, The Ukrainian Academy of Sciences, Kiev, 1962 (in Russian).
[7] O.A. Goroshko, G.N. Savin, Introduction to Mechanics of One-Dimensional Bodies with Variable Length, Naukova Dumka, Kiev, 1971 (in Russian).
[8] Y.A. Mitropolskii, Problems of the Asymptotic Theory of Nonstationary Vibrations, Israel Program for Scientific Translations Ltd., Jerusalem, 1965.
[9] T. Kotera, Vibrations of string with time-varying length, Bulletin of the JSME 21 (1978) 1469–1474.
[10] S. Marczyk, J. Niziol, Transverse–longitudinal vibrations of ropes with time-varying length, Engineering Transactions 27 (1979) 403–415 (in Polish).
[11] A. Klich, The methods of calculations of operating and emergency loads in mine hoists with deep shafts, Selected Problems in Mining and Mechanical Processing 21 (1981) 3–15 (in Polish).
[12] R.R. Mankowski, A Study of Nonlinear Vibrations Occurring in Mine Hoisting Cables, Ph.D. Thesis, Faculty of Engineering, University of the Witwatersrand, Johannesburg, South Africa. 1982.
[13] C.P. Constancon, The Dynamics of Mine Hoist Catenaries, Ph.D. Thesis, Faculty of Engineering, University of the Witwatersrand, Johannesburg, South Africa, 1993.
[14] N.C. Perkins, C.D. Mote Jr., Three-dimensional vibration of travelling elastic cable, Journal of Sound and Vibration 114 (1987) 325–340.
[15] A. Kumaniecka, J. Niziol, Dynamic stability of a rope with slow variability of the parameters, Journal of Sound and Vibration 178 (1994) 211–226.
[16] Y. Terumichi, M. Ohtsuka, M. Yoshizawa, Y. Fukawa, Y. Tsujioka, Nonstationary vibrations of a string with time-varying length and a mass-spring system attached at the lower end, Nonlinear Dynamics 12 (1997) 39–55.
[17] C. Dimitriou, A. Whillier, Vibrations in winding ropes: an appraisal, SAIMechE Hoisting Conference, Johannesburg, South Africa, Paper 34, 1973, pp. 1–13.
[18] M.E. Greenway, A simple static and dynamic analysis of coupled extensional-torsional behaviour of winding rope, Report No. 90-T 22, Anglo American Corporation, Johannesburg, 1990.
[19] H. Hitchen, Ropes for drum and Koepe friction hoists, The Canadian Mining and Metallurgical Bulletin 56 (1963) 122–130.
[20] R.S. Hamilton, M. E. Greenway, A finite element study of the coupled extensional-torsional behaviour of winding ropes Report No. 91-T-16, Anglo American Corporation, Johannesburg, 1991.
[21] G.F. Carrier, On the non-linear vibration problem of the elastic string, Quarterly of Applied Mathematics 3 (1945) 157–165.
[22] D.W. Oplinger, Frequency response of nonlinear stretched string, Journal of the Acoustical Society of America 32 (1960) 1529–1538.
[23] G.S.S. Murthy, B.S. Ramakrishna, Nonlinear character of resonance in stretched strings, Journal of the Acoustical Society of America 38 (1965) 461–471.
[24] J.W. Miles, Stability of forced oscillations of a vibrating string, Journal of the Acoustical Society of America 38 (1965) 855–861.
[25] R. Narasimha, Non-linear vibration of an elastic string, Journal of Sound and Vibration 8 (1968) 134–146.
[26] G.V. Anand, Stability of nonlinear oscillations of stretched strings, Journal of the Acoustical Society of America 46 (1969) 667–677.
[27] T.K. Caughey, Large amplitude whirling of an elastic string—a nonlinear eigenvalue problem, SIAM Journal of Applied Mathematics 18 (1970) 210–237.
[28] P. Hagedorn, B. Schäfer, On non-linear free vibrations of an elastic cable, International Journal of Non-Linear Mechanics 15 (1980) 333–340.
[29] J. Miles, Resonant nonplanar motion of a stretched string, Journal of the Acoustical Society of America 75 (1984) 1505–1510.

[30] C. Gough, The nonlinear free vibration of a damped elastic string, Journal of the Acoustical Society of America 75 (1984) 1770–1776.
[31] J.A. Wickert, C.D. Mote Jr, Classical vibration analysis of axially moving continua, Transactions of the American Society of Mechanical Engineers, Journal of Applied Mechanics 57 (1990) 738–744.
[32] J.G. de Jalon, E. Bayo, Kinematic and Dynamic Simulation of Multibody Systems, Springer, New York, 1994.
[33] M. Géradin, D. Rixen, Mechanical Vibrations. Theory and Application to Structural Dynamics, Wiley, New York, 1994.
[34] N.C. Perkins, Modal interactions in the non-linear response of elastic cables under parametric/external excitation, International Journal of Non-Linear Mechanics 27 (1992) 233–250.
[35] A. Luongo, G. Rega, F. Vestroni, Planar non-linear free vibrations of an elastic cable, International Journal of Non-Linear Mechanics 19 (1984) 39–52.
[36] A. Watzky, Non-linear three-dimensional large-amplitude damped free vibration of a stiff elastic stretched string, Journal of Sound and Vibration 153 (1992) 125–142.
[37] S. Timoshenko, D.H. Young, W. Weaver, Vibration Problems in Engineering, 4th Edition, Wiley, New York; 1974.
[38] D.J. Inman, Engineering Vibration, Prentice-Hall, Englewood Cliffs, NJ, 1996.
[39] S. Kaczmarczyk, The passage through resonance in a catenary-vertical cable hoisting system with slowly varying length, Journal of Sound and Vibration 208 (1997) 243–269.